The Crystal Structure of Phosphonate-Inhibited D-Ala-D-Ala Peptidase Reveals an Analogue of a Tetrahedral Transition State[†,‡]

Nicholas R. Silvaggi,[§] John W. Anderson,[||] Shaun R. Brinsmade,[§] R. F. Pratt,*[,||] and Judith A. Kelly*[,§]

Department of Molecular and Cell Biology and Institute for Materials Science, University of Connecticut, Storrs, Connecticut 06269-3125, and Department of Chemistry, Wesleyan University, Middletown, Connecticut 06459-0180

Received September 24, 2002; Revised Manuscript Received November 12, 2002

ABSTRACT: D-Alanyl-D-alanine carboxypeptidase/transpeptidases (DD-peptidases) are β-lactam-sensitive enzymes that are responsible for the final peptidoglycan cross-linking step in bacterial cell wall biosynthesis. A highly specific tripeptide phosphonate inhibitor was designed with a side chain corresponding to a portion of the *Streptomyces* R61 peptidoglycan. This compound was found to be a slow, irreversible inactivator of the DD-peptidase. Molecular modeling suggested that although a pentacoordinated intermediate of the phosphonylation reaction would not interact strongly with the enzyme, a tetracoordinated phosphonyl enzyme might be analogous to a transition state in the reaction with peptide substrates. To investigate this possibility, the crystal structure of the phosphonyl enzyme was determined. The 1.1 Å resolution structure shows that the inhibitor has phosphonylated the catalytic serine (Ser62). One of the phosphonyl oxygens is noncovalently bound in the oxyanion hole, while the other is solvated by two water molecules. The conserved hydroxyl group of Tyr159 forms a strong hydrogen bond with the latter oxygen atom (2.77 Å). This arrangement is interpreted as being analogous to the transition state for the formation of the tetrahedral intermediate in the deacylation step of the carboxypeptidase reaction. The proximity of Tyr159 to the solvated phosphonyl oxygen suggests that the tyrosine anion acts as a general base for deacylation. This transition state analogue structure is compared to the structures of noncovalent DD-peptidase reaction intermediates and phosphonylated β-lactamases. These comparisons show that specific substrate binding to the peptidase induces a conformational change in the active site that places Ser62 in an optimal position for catalysis. This activated conformation relaxes as the reaction proceeds.

The D-alanyl-D-alanine carboxypeptidase/transpeptidases (DD-peptidases)[1] belong to a family of enzymes known as penicillin binding proteins (PBPs). These enzymes are responsible for the cross-linking of neighboring peptidoglycan strands in the final step of bacterial cell wall biosynthesis (*1*, *2*). Because β-lactams mimic the natural D-Ala-D-Ala substrate of the DD-peptidases, these enzymes are the targets of β-lactam antibiotics such as penicillins and cephalosporins. These drugs inhibit PBPs by forming very long-lived acyl−enzyme intermediates (*3*). The DD-peptidase from *Streptomyces* strain R61, a 37.5 kDa exocellular enzyme, has served extensively as a model for the membrane-bound PBPs that catalyze the majority of cell wall cross-linking (*4*, *5*).

The reaction begins with binding of a peptidoglycan polymer (Figure 1), termed the donor strand, to the enzyme. A nucleophilic serine Oγ atom attacks the carbonyl carbon of the D-Ala−D-Ala peptide bond of the substrate, progressing through a transient tetrahedral transition state to a tetrahedral intermediate. The tetrahedral intermediate collapses through a further transition state to form an acyl−enzyme complex with concomitant release of the terminal D-Ala. Many DD-peptidases are bifunctional enzymes, at least *in vitro*, capable of carboxypeptidase and transpeptidase activity, so the acyl−enzyme complex has two possible fates. First, the acyl−enzyme complex may simply hydrolyze, thereby releasing a peptidoglycan strand shortened by one D-Ala residue. The carboxypeptidase reaction of the R61 DD-peptidase proceeds as follows:

$$E + S \leftrightarrows ES \rightarrow ES^* + P_1 \rightarrow EP_2 \leftrightarrows E + P_2$$

where ES represents the noncovalent Henri−Michaelis complex, ES* the covalent acyl−enzyme intermediate, P_1 free D-alanine, EP_2 the noncovalent complex between the enzyme and the peptidoglycan product of the carboxypeptidation reaction, and P_2 the shortened peptidoglycan product. Alternatively, if a second strand of peptidoglycan is available, the enzyme can form a peptide bond between the first peptidoglycan strand and the glycylamine (left center of

[†] This research was supported in part by grants from the State of Connecticut Critical Technologies Program in Drug Design (to J.A.K.) and from the National Institutes of Health (to R.F.P.).

[‡] Structure submitted to Protein Data Bank (entry 1MPL).

* To whom correspondence should be addressed. R.F.P.: phone, (860) 685-2629; fax, (860) 685-2211; e-mail, rpratt@wesleyan.edu. J.A.K.: phone, (860) 486-4353; fax, (860) 486-4331; e-mail, kelly@uconnvm.uconn.edu.

[§] University of Connecticut.

[||] Wesleyan University.

[1] Abbreviations: DD-peptidase, D-alanyl-D-alanine carboxypeptidase/transpeptidase; ES, enzyme−substrate complex; EPs, enzyme−products complex; ES*, acyl−enzyme intermediate; ES[‡], phosphonylated enzyme.

10.1021/bi0268955 CCC: $25.00
Published on Web 01/14/2003

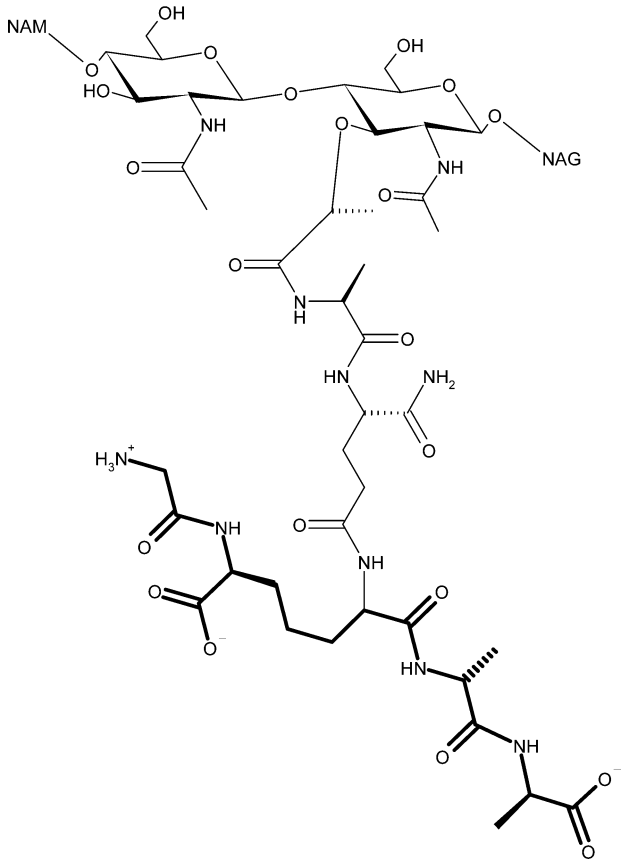

FIGURE 1: Schematic of the *Streptomyces* sp. peptidoglycan monomer. The peptide portion corresponding to the tetrapeptide substrate (**1**) is represented with bold lines.

Figure 1) of the second, resulting in a cross-linked peptidoglycan polymer.

Recent studies with a synthetic tetrapeptide, **1**, that is identical to the C-terminus of the peptide portion of the *Streptomyces* sp. peptidoglycan (Figure 1, bold portion) resulted in the crystallographic structures of two noncovalent complexes, the Henri−Michaelis (ES) and enzyme−products complexes (EPs) (*6*, *7*). The ES complex was trapped using an inactive, cross-linked enzyme.

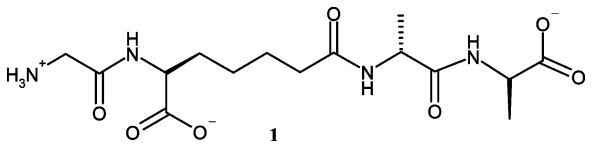

1

The ES structure shows how the active site residues interact with the tetrapeptide substrate to position the scissile peptide bond for nucleophilic attack by the reactive serine Oγ. The EPs complex highlights changes in the positions of active site residues and their noncovalent interactions with the tripeptide product that may play a role in ejecting products from the active site. However, it has not yet been possible to trap covalent intermediates with peptide substrates because the active enzyme is required in this case, and substrates quickly deacylate. A tripeptide phosphonate analogue of **1**, phenyl glycyl-L-α-aminopimelyl-ϵ-(D-2-aminoethyl)phosphonate (**2**), was designed for this purpose. This molecule acts as an irreversible covalent inhibitor of the DD-peptidase, making it possible to trap a tetrahedral transition state analogue (ES‡), which is described herein.

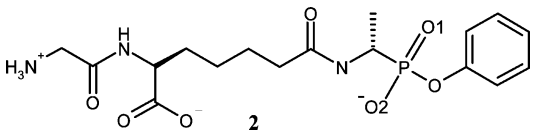

2

In addition to providing information about a tetrahedral transition state, this structure illustrates movements of key active site residues that are important in catalysis. Taken together, the crystal structures of the Henri−Michaelis complex, the phosphonate tetrahedral transition state analogue, and the enzyme−products complex provide detailed structural information about each of the steps in the kinetic mechanism of the R61 DD-peptidase.

MATERIALS AND METHODS

*Phenyl Glycyl-L-α-aminopimelyl-ϵ-(D-2-aminoethyl)phosphonate (**2**).* D-2-[*N*-(Benzyloxycarbonyl)amino]ethylphosphonic acid was prepared in a previously described fashion (*8*). This compound was converted to its phenyl ester by the procedure of Markowska et al. (*9*). The dry phosphonic acid (0.94 g, 3.7 mmol) was dissolved in pyridine (50 mL) that had been freshly distilled from barium oxide. Triphenyl phosphite (2.1 mL, 11 mmol, 3 equiv) was added and the solution heated under reflux in a nitrogen atmosphere for 8 h. The reaction mixture was then evaporated to dryness under vacuum, the residue dissolved in water, and the solution extracted three times with ethyl acetate. The aqueous solution was then freeze-dried to give the product (1.0 g, 81%) as a colorless solid that was used without further purification [^{1}H NMR (^2H_2O) δ 1.33 (3H, dd, J = 9, 15 Hz, CH_3), 3.93 (1H, m, CH), 4.96 (2H, s, CH_2), 7.08 (3H, m, ArH), 7.23 (2H, m, ArH), 7.25 (5H, br s, ArH)]. The amine, phenyl D-2-aminoethylphosphonate, was then obtained by catalytic hydrogenation as follows. The protected amine (1.0 g) in methanol (10 mL) with Pd/C (10%, 50 mg) was hydrogenated under 40 psi hydrogen gas for 24 h. The reaction mixture was filtered through a Celite pad and the filtrate evaporated to dryness. The residue was purified by Dowex 50X4-200 cation exchange chromatography with elution by a 0 to 2 M aqueous ammonia gradient. The colorless solid product was obtained in 30% yield [^{1}H NMR (^2H_2O) δ 1.55 (3H, dd, J = 8, 16 Hz, CH_3), 3.60 (1H, m, CH), 7.21 (3H, m, ArH), 7.43 (2H, m, ArH)]. The amine was then coupled to *N*-(benzyloxycarbonyl)glycyl-L-α-aminopimelic acid α-benzyl ester (*6*) by a variation of the method of Ho et al. (*10*). The pimelic acid (100 mg, 0.22 mmol) was dissolved in dimethylformamide (1 mL) and the solution cooled, with stirring, on ice. The amine (43 mg, 0.22 mol) was dissolved in water (0.5 mL) and added to the previous solution. To this mixture was added triethylamine (64 μL, 0.43 mmol), followed by 1-hydroxybenzotriazole (43 mg, 0.22 mmol) and, finally, 1-[3-(dimethylamino)propyl]-3-ethylcarbodiimide (91.5 mg, 0.43 mmol). The reaction mixture was stirred for 15 h at 5 °C and then evaporated to dryness under vacuum and the residue purified by Sephadex QAE A25 anion exchange chromatography by elution with a 0 to 2 M gradient of aqueous triethylammonium bicarbonate. The coupled product

was obtained as a colorless triethylammonium salt in 66% yield [^{1}H NMR (^2H_2O) δ 1.29 (3H, dd, $J = 9$, 15 Hz, CH_3), 1.43 (2H, m, γ-CH_2), 1.66 (2H, m, δ-CH_2), 1.74 (2H, m, β-CH_2), 2.07 (2H, ABq, $J = 7$ Hz, ϵ-CH_2), 3.76 (2H, s, Gly CH_2), 4.20 (1H, m, CH), 4.30 (1H, m, CH), 5.08 (2H, s, CH_2O), 5.14 (2H, ABq, $J = 12$ Hz, CH_2O), 7.08 (3H, m, ArH), 7.29 (2H, m, ArH), 7.39 (10H, m, ArH)].

The final product **2** was then obtained by hydrogenation (40 psi hydrogen gas) of its *N*-benzyloxycarbonyl benzyl ester derivative (120 mg, 0.14 mmol) in methanol (10 mL) over Pd/C (10%, 50 mg) for 24 h at room temperature. The reaction mixture was then filtered through a Celite pad and the filtrate evaporated to dryness. The product, a colorless triethylammonium salt (31 mg, 40%), was purified by Sephadex G-10 column chromatography in water [^{1}H NMR (^2H_2O) δ 1.33 (3H, dd, $J = 6$, 18 Hz, CH_3), 1.58 (2H, m, γ-CH_2), 1.73 (2H, m, δ-CH_2), 1.83 (2H, m, β-CH_2), 2.22 (2H, t, $J = 7$ Hz, ϵ-CH_2), 3.77 (2H, ABq, $J = 18$ Hz, Gly CH_2), 4.22 (1H, m, CH), 4.30 (1H, m, CH), 7.16 (3H, m, ArH), 7.37 (2H, m, ArH); ESMS *m*/*e* 416.3 (M + 1)]. Alkaline hydrolysis of **2** yielded 1 equiv of phenol, determined spectrophotometrically.

*Phenyl N,N′-Diacetyl-L-lysyl-D-2-aminoethylphosphonate (**3**).* *N*,*N*′-Diacetyl-L-lysine (24.5 mg, 0.15 mmol) and phenyl D-2-aminoethylphosphonate (30 mg, 0.15 mmol) were carbodiimide-coupled as described above. The product was purified by a succession of steps involving Dowex 50X4-200 cation exchange, Sephadex G-10 size exclusion, Sephadex QAE A25 anion exchange, and, finally, Biogel P2 size exclusion chromatography. The final product, a colorless potassium salt, was obtained in 22% yield (15 mg) [^{1}H NMR (^2H_2O) δ 1.35 (3H, dd, $J = 9$, 18 Hz, CH_3), 1.38 (2H, m, γ-CH_2), 1.49 (2H, m, δ-CH_2), 1.69 (2H, m, β-CH_2), 1.95 (3H, s, Ac), 2.04 (3H, s, Ac), 3.13 (2H, t, $J = 6$ Hz, ϵ-CH_2), 4.22 (1H, m, CH), 4.29 (1H, m, CH), 7.13 (2H, m, ArH), 7.21 (1H, m, ArH), 7.38 (2H, m, ArH); ESMS *m*/*e* 412.4 (M + 1)]. Alkaline hydrolysis of **3** also yielded 1 equiv of phenol, determined spectrophotometrically.

Inhibition Kinetics. Enzyme purified as described in ref *11* was provided by J.-M. Frère of the Université de Liège (Liège, Belgium). All solutions of enzymes, phosphonates, and substrates were prepared in 20 mM MOPS buffer (pH 7.5). Inhibition experiments were carried out in this buffer at 25 °C. Incubation mixtures (25 μL) containing the R61 DD-peptidase (6.8 μM) and phosphonate (5 mM) were set up. Aliquots (2 μL) of these were taken and added to cuvettes containing 298 μL of a solution of the substrate *m*-{[(phenylacetyl)-D-alanyl]oxy}benzoic acid (*12*). Initial rates of hydrolysis of the latter were monitored spectrophotometrically at 290 nm. These were determined as a function of the time of incubation. Pseudo-first-order rate constants of inactivation, k_{obs1}, were obtained from these data by means of a nonlinear least-squares program; Scheme 1 was assumed.

Scheme 1

$$E + I \underset{K_i}{\rightleftharpoons} EI \xrightarrow{k_i} EI'$$

From the measured rate constant at 5 mM phosphonate and the K_i value determined as described below, a k_i value could be calculated from eq 1, where [I] is the phosphonate concentration.

$$k_{obs1} = k_i[I]/([I] + K_i) \quad (1)$$

The ability of **2**, **3**, and the alkaline hydrolysis product of the former, **5**, to quickly and reversibly inhibit the DD-peptidase was also determined. To do this, the acylation of the peptidase (0.55 μM) by dansylpenicillin (*13*) (0.15 mM) was monitored by means of the fluorescence emission intensity decrease at 320 nm on excitation at 280 nm. This experiment was repeated in the presence of **2** (0−4 mM), its hydrolysis product **5** (0−1.24 mM), and **3** (5 mM). Pseudo-first-order rate constants, k_{obs2}, were obtained by fitting these progress curves to an exponential function by means of a nonlinear least-squares program. From the k_{obs2} values as a function of the phosphonate concentration, K_i values were obtained using eq 2 which assumes simple competitive inhibition

$$k_{obs2} = k^0_{obs2}/(1 + [I]K_i) \quad (2)$$

where k^0_{obs2} is the acylation rate in the absence of phosphonate, [I] is the phosphonate concentration, and K_i is the inhibition constant. Essentially no irreversible inactivation of the enzyme by phosphonate took place on the time scale of these experiments.

Crystallographic Data Collection. R61 DD-peptidase was crystallized by the hanging drop vapor diffusion method from a solution containing 20 mg/mL enzyme, 15% polyethylene glycol (PEG) 8000, and 50 mM sodium phosphate (pH 6.8) over a reservoir containing 20% PEG 8000 and 50mM sodium phosphate. A 0.78 mm × 0.2 mm × 0.1 mm crystal (space group $P2_12_12_1$, cell dimensions of $a = 50.9$ Å, $b = 66.8$ Å, and $c = 100.0$ Å, one 37.5 kDa molecule per asymmetric unit) was soaked for 14 days in 2.9 mM phosphonate, 28% PEG 8000, 5% glycerol, and 50 mM sodium phosphate (pH 6.8). The crystal was transferred into a cryoprotectant solution consisting of the soaking solution with 10% glycerol for 30 s and then into a cryoprotectant with 20% glycerol for 30 s and finally flash-cooled in a gaseous nitrogen stream at 95 K. Data were collected on beam line X12B at the National Synchrotron Light Source (Brookhaven National Laboratory, Upton, NY) and processed using the HKL package (*14*).

Structure Refinement. Initial refinement was carried out using CNS (*15*) to 1.5 Å resolution. The refined model was fitted to $2|F_o| - |F_c|$ and $|F_o| - |F_c|$ electron density maps in XTALVIEW (*16*). Solvent molecules with reasonable hydrogen bond distances and geometry were added, except in the active site. Once refinement of the model reached an *R* factor of 0.18, further refinement was performed in SHELX-97 (*17*). The model was refined at full resolution (1.12 Å) before performing anisotropic refinement, which resulted in a drop of 0.029 in both *R* and R_{free}. Further rounds of fitting and refinement were performed, adding additional solvent molecules and alternate conformations for discretely disordered residues. When the *R* factor converged at 0.145, the inhibitor molecule was modeled and refined. When the *R* factor converged at 0.117, hydrogen atoms were added that appeared as 3σ peaks in $|F_o| - |F_c|$ electron density maps, with good geometry for hydrogen bonding.

Table 1: Rate Constants for Inhibition of β-Lactam-Recognizing Enzymes by Phosphonates

enzyme	phosphonate	k_i/K_i[a] (s^{-1} M^{-1})
R61 DD-peptidase	**2**	0.10 ± 0.01
	3	*b*
	4	*b*
P99 β-lactamase	**2**	$(1.4 \pm 0.3) \times 10^{-2}$
	3	*b*
	4	258

[a] Parameters of Scheme 1. [b] No inhibition observed.

RESULTS AND DISCUSSION

Characterization of the Phosphonate Inhibitor. The phosphonate ester **2** was designed as a specific inhibitor of the R61 DD-peptidase and, for this purpose, has the *N*-glycyl-L-α-aminopimelyl side chain of the *Streptomyces* R61 cell wall substrate. The R61 active site is specific for this side chain as revealed by structural and kinetic studies of substrate **1** (*6*, *7*). Table 1 gives data that show the rates of inhibition of the peptidase and the structurally similar (*18*) class C β-lactamase of *Enterobacter cloacae* P99 by phosphonates **2**−**4**.

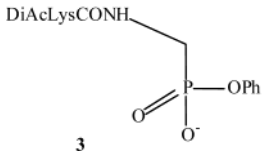

3

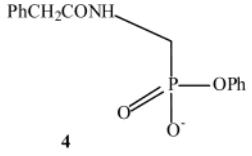

4

Phosphonate **4**, previously studied (*19*), has a side chain favored by β-lactamases. The interesting features of these data are the following. First, as reported previously (*20*), phosphonates such as **4**, with side chains favorable to β-lactamases, do not inhibit the DD-peptidase. Further, phosphonate **3**, which has the side chain of the generic small molecule amide substrate of DD-peptidases, *N*,*N*′-diacetyl-L-lysyl-D-alanyl-D-alanine, also does not noticeably inhibit the peptidase. This presumably reflects the relatively low specificity of this peptide for the enzyme ($k_{cat}/K_m = 5500$ s^{-1} M^{-1}). On the other hand, **2**, which has the specific side chain of the excellent peptide substrate **1**, does inhibit the peptidase, albeit slowly (Table 1). It is also interesting that neither **2** (3.3 mM) nor **3** (5 mM) had appreciable inhibitory action against the β-lactamase. This suggests that there is greater side chain specificity in phosphonate inhibitors of β-lactamases than has been evident to date. It is known, however, that the *N*,*N*′-diacetyl-L-lysyl side chain on a β-lactam produces both a poorer P99 β-lactamase substrate and a poorer R61 DD-peptidase inhibitor than does the phenylacetyl side chain of **4** (*21*).

Despite the slow inactivation of the peptidase produced by **2**, evidence was obtained for its noncovalent binding to the enzyme. Studies of inhibition of dansylpenicillin inactivation of the peptidase by **2** led to a K_i (Scheme 1) value of 2.1 ± 0.2 mM. This binding, although weak compared to that of **1** (8 μM), must reflect the influence of the side chain. Noncovalent binding, even to this degree, has not been previously observed, for example, in the reaction of phenylacetylglycylphosphonates such as **4** with the P99 β-lactamase, although these compounds rapidly inhibit this enzyme (*19*). Loss of the leaving group from **2** improves the binding to the R61 DD-peptidase; the K_i value for **5**, the hydrolysis product of **2**, was found to be 0.17 ± 0.3 mM, a value similar to that of **6** (0.16 mM), the hydrolysis product of peptide **1**.

Table 2: Crystallographic Data

resolution limit (Å)	1.12
no. of reflections	
measured	701505
unique	127013
$F > 4\sigma$	106900
completeness (%)	
all data	96.6
highest-resolution shell (1.16−1.12 Å)	75.1
R_{sym}[a] (on I)	0.041
$I/\sigma(I)$	
overall	27.2
highest-resolution shell	3.0
refinement	
resolution (Å)	∞−1.12
R factor (all data)	0.113
R free	0.139
data in test set	6242
no. of non-hydrogen atoms	3132
no. of hydrogen atoms	189 (5.3%)
rms deviation	
bond lengths (Å)	0.015
bond angles (deg)	2.50
average B factor (all atoms) (Å^2)	12.7
average B factor of ligand (Å^2)	8.2

[a] $R_{sym} = \sum|I_{obs} - \langle I\rangle|/\sum\langle I\rangle$.

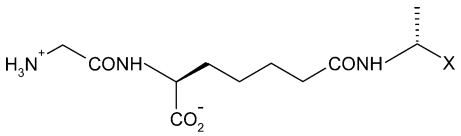

5, X = PO_3H^-
6, X = CO_2^-

The crystal structure of the EPs complex has shown that the *N*-glycyl-L-α-aminopimelyl side chain of **6** binds to the enzyme exactly as does that of **1** itself, although the penultimate D-Ala carboxylate group disrupts the catalytic center (*7*).

The much poorer activity of phosphonate inhibitors in general against the DD-peptidase than against the β-lactamase, even when specific side chains are present, is notable in view of the very similar active sites of these enzymes. Molecular modeling (R. F. Pratt and J. W. Anderson, unpublished observations) suggested that this difference arises from the poorer fit of the pentacoordinated phosphorus intermediate into the DD-peptidase active site. This, in turn, seems to be the result of a significant difference between the two classes of enzymes in the overall shape of the active site (*22*). On the other hand, models of tetrahedral phosphonate adducts suggested that these fitted equally well into the two types of active sites and thus that these structures may represent good transition state analogues (*23*). Crystallographic examination of the DD-peptidase−phosphonate complex was therefore undertaken.

Structure of the Phosphonylated DD-Peptidase. The structure of the R61 DD-peptidase complexed with **2** has been determined to 1.1 Å resolution and refined to a crystallographic R factor of 0.113 for all data (Table 2, PDB entry 1MPL). Difference Fourier methods were employed to study the complex using the native enzyme phases (3PTE). Electron density for the tripeptide phosphonate was interpretable even in the earliest stages of refinement, but the inhibitor was not modeled until the R factor reached 0.145.

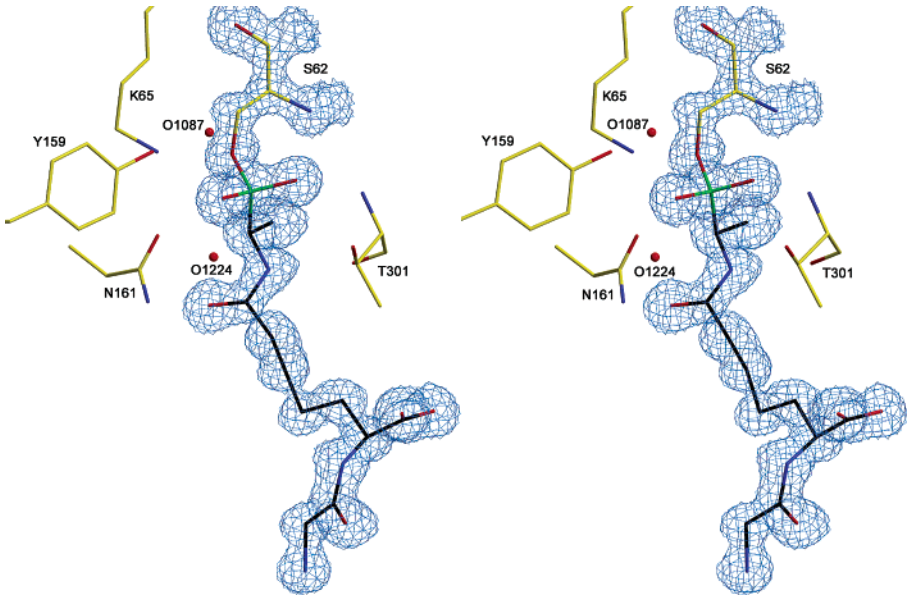

FIGURE 2: Stereoview of $2|F_o| - |F_c|$ electron density contoured at 1σ showing the covalent linkage between the inhibitor phosphorus atom (green) and Ser62 Oγ. Electron density and stick residues generated using XTALVIEW (*16*) and complete image rendered using RASTER3D (*36*). Carbon atoms of active site residues are yellow, while those of the inhibitor are black.

Table 3: Phosphonylated Serine Geometry in the R61 DD-Peptidase ($ES^{\ddagger}$), the Class A β-Lactamase of *S. aureus* PC1, and the Class C β-Lactamase of *E. cloacae* P99

	$ES^{\ddagger}$	PC1	P99
	Distances (Å)		
Ser Oγ−P	1.60	1.61	1.64
P−O1	1.49	1.42	1.55
P−O2	1.48	1.45	1.56
P−C	1.82	1.81	1.55
	Dihedral Angles (deg)		
Ser Cβ−Oγ−P−O1	−47	−24	−59
Ser Cβ−Oγ−P−C	−163	−155	−165
Ser Oγ−P−C−N	177	177	36

The position of the phosphonate in this structure is best interpreted as a tetrahedral transition state analogue. There is continuous electron density between the phosphorus atom of the inhibitor and Ser62 Oγ, even at the 2σ level, indicating a covalent bond between these two atoms (Figure 2). The distance between the inhibitor P and Ser62 Oγ is 1.6 Å (Table 3), which is the average for the P−O bonds in phosphate (*24*). The phosphorus atom adopts a tetrahedral geometry with O1 (see **2**) interacting with the oxyanion hole formed by the main chain amides of Ser62 (2.75 Å) and Thr301 (2.70 Å), while O2 is solvated by two water molecules, O1087 (2.87 Å) and O1224 (2.81 Å) (Figure 3).

The tripeptide portion of molecule **2** binds antiparallel to the B3 β-strand [numbering as defined by Kelly et al. (*25*)], making a number of strong interactions with active site residues (Figure 3). The D-Ala amide forms a strong hydrogen bond to the Thr301 carbonyl oxygen (2.79 Å), and the L_1-α-carbonyl of the diaminopimelic acid moiety interacts with Nδ of the highly conserved Asn161 (2.88 Å). Lying across the hydrophobic surface formed by Phe120 and Trp233 are the four methylene groups of the diaminopimelate. The N-terminal portion of the tripeptide is securely bound in the substrate specificity subsite of the active site described by McDonough et al. (*7*).

The positions of active site functional groups around the phosphonyl group of the inhibitor indicate that the present structure, which we interpret as **7**, is analogous to a tetrahedral transition state (**8** or **9**) in the deacylation reaction. The complex isolated crystallographically must be associated with the deacylation step rather than acylation because of the absence of the leaving group on **2**. The Tyr159 OH group is within hydrogen bonding distance of both Ser62 Oγ and the solvated phosphonyl oxygen, O2 (2.90 and 2.77 Å, respectively). However, only the phosphonyl oxygen is at a suitable angle for hydrogen bonding ($159^{C\zeta}-159^{OH}-O2$ angle of 110.1° vs $159^{C\zeta}-159^{\circ OH}-62^{O\gamma}$ angle of 154.4°). Thus, it seems from this structure that Tyr159, as the phenoxide anion, would act as a general base in deacylation, activating a deacylating water molecule for attack on the carbonyl carbon of the acyl−enzyme intermediate as in **8**. A positive charge on Lys65 would serve both to stabilize the phenoxide anion on Tyr159 and, through its proximity to Ser62 Oγ, to polarize the ester C−O bond for nucleophilic attack by the deacylating water molecule. This scenario would, by symmetry, suggest that Tyr159 is the general acid catalyst for breakdown of the tetrahedral intermediate in acylation, i.e., responsible for protonation of the D-Ala leaving group in the transpeptidation reaction. Without movement of the functional groups, this would also suggest that neutral Lys65 would be the general base catalyst in formation of the tetrahedral intermediate in acylation and the general acid in breakdown of the tetrahedral intermediate in deacylation (**9**), but given the likely mobility of these functional groups, Tyr159 could also perform these roles (e.g., **10**).

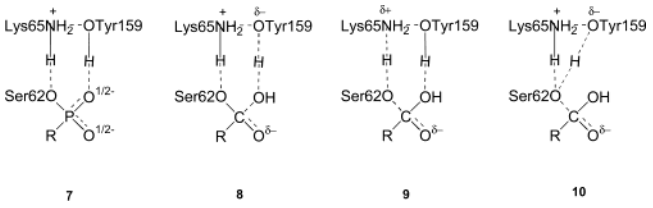

7 8 9 10

Comparison with the Native DD-Peptidase Structure. Least-squares fitting of the coordinates of the phosphonylated DD-

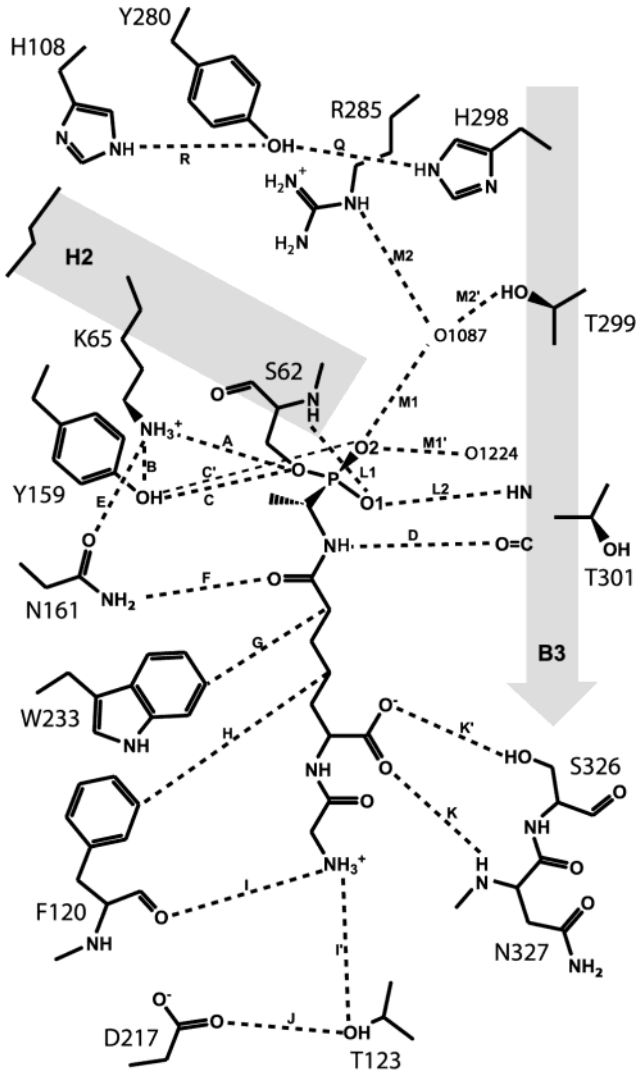

FIGURE 3: Schematic of the R61 active site showing residue−inhibitor and residue−residue distances given in Table 5, as well as the relative positions of key secondary structural elements, as defined by Kelly et al. (*25*). The B3 β-strand is represented by an arrow and the H2 helix by a rectangle.

peptidase to those of the native enzyme (*25*) results in an rms difference of 0.620 Å for all 146 atoms in the 16 active site residues (Table 4). The low rms difference indicates that there is relatively little change in the positions of active site residues upon binding the phosphonate molecule. Indeed, only Ser62 shifts significantly from its native position upon phosphonylation of the enzyme. The α-carbon of this residue is displaced toward Lys65 and Tyr159 by 0.65 Å. Lys65 and Tyr159, which in the native structure each adopt two alternate conformations (Figure 4), are both stabilized in single conformations in the ES‡ complex, overlaying Lys65A and Tyr159A of the native enzyme almost exactly. With Lys65 and Tyr159 both fixed, the movement of Ser62 evident in the ES‡ complex places serine Oγ 2.82 Å away from lysine Nζ, and 2.89 Å away from the tyrosine hydroxyl (A and C in Table 5 and Figure 3). In the native structure, these distances are 4.13 and 3.76 Å, respectively (Table 5). The interaction of Lys65 Nζ with the Tyr159 hydroxyl (B in Table 5 and Figure 3) is weakened slightly upon formation of the complex, while lysine Nζ interacts more strongly with Asn161 Oδ (E in Table 5 and Figure 3) in the complex than it does in the native structure.

Table 4: Least-Squares Fitting of Native DD-Peptidase and Covalent and Noncovalent Complexes

reference model	mobile model	rmsd		S62 Cα distance[a,b] (Å)
		AS[c]	60−75[d]	AS
native (3PTE)	ES (1IKG)	0.71	0.21	0.84
	ES‡ (1MPL)	0.35	0.17	0.65
	EPs (1IKI)	0.47[e]	0.11	0.37

[a] S62 Cα distance refers to the distance between S62 Cα in the reference and mobile models. [b] Resolutions and estimated standard deviations in atomic coordinates (in angstroms) of the four structures are as follows: 1.6 and 0.14 for the native structure, 1.9 and 0.15 for ES, 1.1 and 0.06 for ES‡, and 1.25 and 0.06 for EPs, respectively. Standard deviations in atomic coordinates were estimated using the method of Luzzati (*35*). [c] Least-squares fitting was performed with the program XTALVIEW using all atoms in the 16 important active site residues [S62, K65, H108, F120, T123, Y159, N161, D217, W233, Y280, R285, H298, T299, T301, S326, and N327 (146 total atoms)]. [d] Least-squares fitting was performed on all main chain atoms from V60 to L75 on helix H2. [e] Alternate conformations of Lys65 and Tyr159 in the native structure, and Thr301 and Ser62 in the EPs structure, were omitted from fitting.

Table 5: Distances in the Native Enzyme (E), the Enzyme−Substrate Complex (ES), the Phosphonate Tetrahedral Transition State (ES‡), the Enzyme−Products Complex (EPs), the Class A β-Lactamase of *S. aureus* PC1,[a] and the Class C β-Lactamase of *E. cloacae* P99

distance (Å)[b]	E[c]	ES	ES‡	EPs	PC1	P99
A	4.13	4.08	2.82	2.74	2.79	3.32
B	2.76	3.27	2.85	2.87	4.05	2.77
C	3.76	3.17	2.89	2.59	3.22	3.00
C′			2.77		3.32	3.40
D		2.88	2.79	2.65	3.56	2.71
E	4.23	4.77	2.77	2.78	2.58	2.57
F		2.79	2.88	2.84	2.61	3.24
G		3.58	3.82	4.47		
H		3.49	3.51	3.30		
I		2.59	2.76	2.68		
I′		2.84	2.71	2.70		
J	2.69	2.58	2.63	2.55		
K		2.91	2.88	2.83		
K′		2.54	2.56	2.56		
L1		2.72	2.75		2.94	3.04
L2		2.79	2.70		2.93	2.29
M1			2.87		3.03	
M1′			2.81			3.22
M2			2.83			
M2′			2.90			
R	3.37	4.10	3.09	3.12		
Q	2.71	2.77	2.72	2.69		

[a] Equivalent residues in DD-peptidases and class A and C β-lactamases are S62, -70, and -64; K65, -73, and -67; Y159, S130, and Y150; and N161, -132, and -152, respectively. [b] Refer to Figure 3 for distances. [c] 'A' conformations of K65 and Y159 used in measurements.

In both structures, water molecule O1087 is held by interactions with Arg285 Nη and Thr299 Oγ (M2 and M2′, respectively, in Table 5 and Figure 3). The interactions with this water molecule become stronger upon formation of the tetrahedral transition state analogue (Table 5). In the phosphonylated enzyme, O1087 solvates one of the phosphonyl oxygens, O2 (Figure 3).

Comparisons with the Enzyme−Substrate and Enzyme−Products Complexes. The tetrahedral transition state analogue was also compared with the Henri−Michaelis complex (ES), and the enzyme−products complex (EPs) structures (*7*). The coordinates for all atoms in the 16 active site residues of the two noncovalent complexes (ES and EPs) were fitted

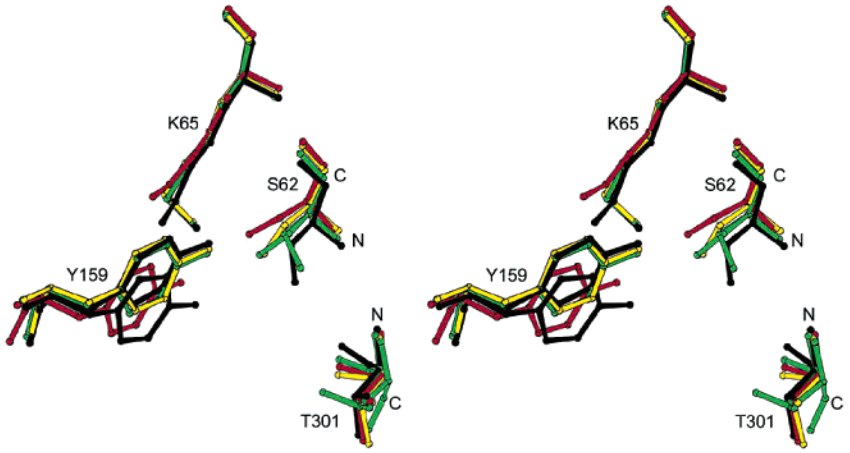

FIGURE 4: Stereoview of four overlaying residues from the native, ES, ES‡, and EPs structures found to be mobile over the course of catalysis. Native residues are black, those of ES red, those of ES‡ yellow, and those of EPs green. This figure was generated with MOLSCRIPT (*37*).

onto the coordinates of the same residues in the tetrahedral transition state analogue. The phosphonylated structure is most similar to the enzyme−products complex, with an rmsd for all atoms in the 16 active site residues of 0.55 Å, compared to 0.62 Å for the native and 0.63 Å for the ES complex. This supports the suggestion made above that the phosphonate-inhibited structure is an analogue of a tetrahedral transition state in the deacylation reaction. Care must be taken when using the coordinates of the active site of the ES complex in comparisons, since the enzyme in this case has been inactivated by covalent cross-links between Lys65, His108, and Tyr159, which effect the positions of these residues (rmsd from native for all 32 atoms in the three residues of 1.21 Å).

Comparison of the three complex structures (ES, ES‡, and EPs) reveals that only four key residues change position over the course of the reaction (Ser62, Lys65, Tyr159, and Thr301). Of these four, only Ser62, Lys65, and Tyr159 seem to be directly involved in catalysis. Mutation of Thr301 to Ile or Ser has only a minor effect on the enzyme activity (*26*), indicating that the side chain of this residue is not crucial for catalysis. It is notable that the tetrapeptide substrate, tripeptide phosphonate inhibitor, and tripeptide product all adopt very similar conformations in the active site. The N-terminal glycine and L-α-carboxylate of the ligands are crucial for tight binding to the enzyme (*6*). Thus, it is not surprising that this portion of the molecule in all three complex structures overlays exactly. Likewise, the residues interacting with this portion of the ligand are also identical in the three structures.

It is interesting to note that O1 and O2 of the phosphonate overlay, respectively, the terminal D-Ala amide nitrogen atom and the penultimate D-Ala carbonyl oxygen of the tetrapeptide substrate. However, because of its tetrahedral geometry and the covalent linkage to Ser62, the inhibitor P is positioned 0.49 Å closer to Ser62 Oγ, relative to the penultimate D-Ala carbonyl C of the tetrapeptide substrate.

Lys65 and Tyr159, two of the four active site residues that move significantly during catalysis, are mobile in the native enzyme, as evidenced by their multiple conformations. However, once substrate binding has taken place, each is stabilized in a conformation corresponding to the 'A' conformer in the native structure (Figure 4). Movement of Thr301 is only apparent in the EPs structure, where the whole residue, including its main chain, takes on an alternate conformation. This movement is thought to play a role in ejection of products from the active site after catalysis (*7*).

The most striking and catalytically significant movement in the enzyme is the relocation of Ser62 that occurs upon substrate binding. Ser62 is located on the first turn of helix H2, the longest helix in the enzyme. While the bulk of H2 has ideal α-helical geometry, the first turn has 3_{10} geometry. Least-squares fitting the three complex structures onto the native structure shows that the entire turn of 3_{10}-helix from Val60 to Thr64 in the ES, ES‡, and EPs structures is displaced relative to the native enzyme (Table 4), while the remainder of H2 is identical in all four structures. These movements are significant given the estimated standard deviations in atomic positions for each structure (see Table 4). The first turn of H2 is most distorted in the Henri−Michaelis complex, with Ser62 Cα displaced by 0.84 Å relative to the native position (Figures 4 and 5). In the phosphonylated enzyme, Ser62 Cα is moved 0.65 Å from the native position. Finally, this turn of helix is more native-like in the EPs complex, with Ser62 Cα displaced by only 0.37 Å. Also interesting is the disposition of Ser62 Oγ in each of these structures. Again, the greatest distortion is seen in the ES complex, where the χ_1 dihedral angle (N−Cα−Cβ−Oγ) is rotated −65°, moving Ser62 Oγ 2.4 Å from its native position. In the ES‡ structure, the χ_1 dihedral angle is rotated −50° with respect to the native enzyme, resulting in a 1.62 Å movement of Ser62 Oγ. Finally, Ser62 in the EPs structure exhibits two alternate conformations. Since the occupancy of the tripeptide product refined to 70%, Ser62 takes on one conformation in the product-bound state, and a second conformation in the non-product-bound state. In the B conformation, which is the product-bound form, χ_1 is rotated by 30°, putting Oγ 0.85 Å from its native position. The degree of movement seen here highlights the mobility of this catalytic center.

The relocation of the 3_{10} turn of helix places further strain on this element of secondary structure that has less ideal hydrogen bonding than that seen in an α-helix. The energy required for this arrangement must be compensated by the

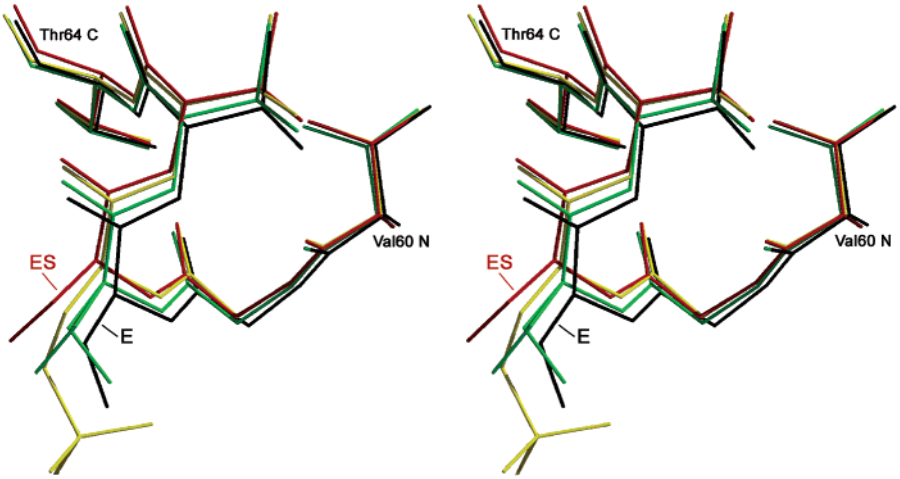

FIGURE 5: Stereoview highlighting the mobility of the 3_{10} turn of helix H2 from Val60 to Thr64. The black model is the native enzyme, the red the ES complex, the yellow ES‡, and the green the EPs complex.

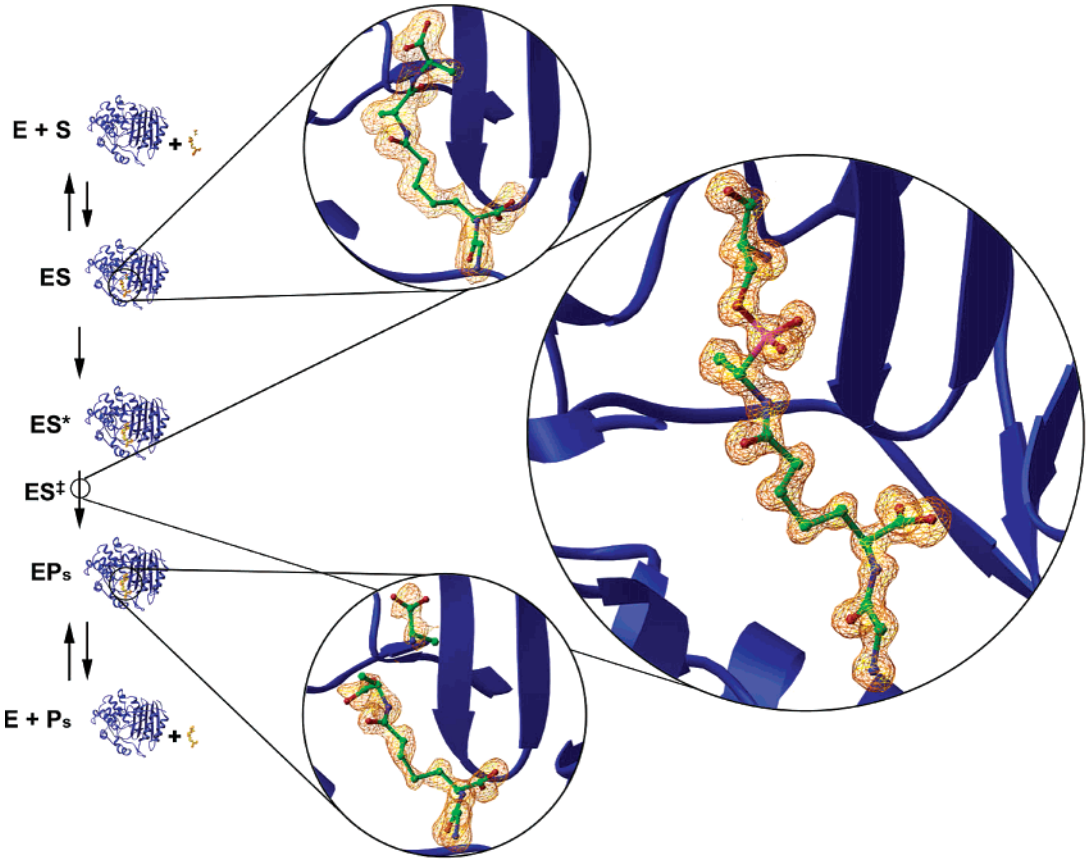

FIGURE 6: Structural representation of the four steps in the carboxypeptidase reaction pathway of the *Streptomyces* R61 DD-peptidase. The ribbon diagrams to the right of each step in the pathway were generated from crystallographic structures of molecules that represent that step. E is represented by the native structure (3PTE). The ES (1IKG) and EPs (1IKI) structures were determined previously by McDonough et al. (*7*). ES‡ (1MPL) was determined in the work presented here. The expanded views show $|F_o| - |F_c|$ electron density for the ES substrate complex (top, 3.0σ contour level), the ES‡ tetrahedral transition state analogue (middle, 3.0σ), and EPs (bottom, 2.5σ). This figure was prepared using RIBBONS (*38*).

binding of substrate in an induced fit fashion. By moving the turn of 3_{10}-helix, and increasing the torsion about χ_1 of the Ser62 side chain, substrate binding places the catalytic serine hydroxyl group very close to Lys65 and Tyr159, which in turn leads to activation of the enzyme for catalysis. The dislocation of the 3_{10} turn of helix. This is supported by the observation that mutation of either Lys65 or Tyr159 results in severely impaired enzyme activity (*27*, *28*). Also, both Tyr159 (or its serine equivalent) and Lys65 are conserved among all serine DD-peptidases and β-lactamases (*28*, *29*). This fact, together with the fact that both the *Streptomyces* K15 DD-peptidase and PBP2x from *Streptococcus pneumoniae* have their catalytic serine residue located on a turn of 3_{10}-helix, supports the notion that movement of this structural element driven by substrate binding may generally play a role in catalysis. Nonspecific peptide substrates, e.g., *N*,*N*′-

diacetyl-L-lysyl-D-alanyl-D-alanine, may be poorer substrates because they lack sufficient specific interactions for inducing the conformational change in this turn of helix.

The DD-peptidases thus appear to represent very nice examples of induced fit enzymes (*30*). Maximum displacement of the 3_{10} turn of helix occurs on formation of the ES complex. Upon formation of the tetrahedral transition state analogue, the turn of 3_{10}-helix relaxes to a position closer to native than that in the noncovalent ES complex. However, Ser62 Cα is still displaced by 0.65 Å relative to the native position (estimated standard deviation of atomic positions 0.14 Å for native and 0.06 Å for the ES‡ complex). After catalysis, this turn of helix relaxes even further, with Ser62 Cα displaced by only 0.35 Å in the EPs complex (esd of atomic positions 0.06 Å). Thus, the straining and relaxation of this 3_{10} turn of helix may act not only to position Ser62 Oγ for activation but also to destabilize the acyl−enzyme and enzyme−products complexes.

Comparisons with Phosphonylated β-Lactamases. β-Lactamases are thought to have evolved from the DD-peptidases (*31*, *32*). The β-lactamases are similar to DD-peptidases in that they bind to and are acylated by β-lactam antibiotics; however, instead of the long-lived acyl−enzyme complexes formed by DD-peptidases, acyl−enzyme intermediates of β-lactamases with β-lactams quickly hydrolyze to regenerate the native enzyme. A number of striking similarities are apparent in comparisons of this DD-peptidase ES‡ structure to phosphonylated class A and class C β-lactamases. Comparisons can be made to the structures of the phosphonate complexes of the class A β-lactamase from *S. aureus* PC1 with *p*-nitrophenyl [(*N*-benzyloxycarbonyl)amino]-methyl phosphonate (1BLS), and the class C β-lactamase from *E. cloacae* P99 with *m*-carboxyphenyl ({*N*-[(*p*-iodophenyl)acetyl]amino}methyl)phosphonate (1BLH). In the phosphonylated class A enzyme, the geometry of the phosphonylated serine residue is very similar to that in the ES‡ complex (Table 3). The Cβ−Oγ−P−C dihedral angles in both structures align the inhibitors antiparallel with the B3 β-strand. The distances between the phosphonate inhibitors in these two structures and three conserved active site residues are also similar (Table 5 and Figure 3).

In contrast, the geometry of the phosphonylated class C β-lactamase, while similar, differs significantly from that of the DD-peptidase (Table 3). The largest difference is in the Oγ−P−C−N dihedral, which places the phosphonate in the P99 structure nearly perpendicular to the B3 β-strand.

These similarities and differences can be explained most easily in terms of substrate specificity. Both the DD-peptidase and the class A enzyme have high substrate specificities. This is reflected in the configuration of the active sites of these enzymes, both of which have relatively occluded active sites near the bottom of the B3 β-strand. The class C enzyme, on the other hand, is a broad spectrum β-lactamase and possesses an extremely open active site, capable of accepting a variety of substrates (*33*). On the basis of substrate−inhibitor profiles and sequence comparisons (*34*), class C β-lactamases are considered to be more closely related to the R61 DD-peptidase than are the class A enzymes. However, the positioning of the phosphonates in these structures (R61, PC1, and P99) shows the phosphonate conformation in the class A PC1 active site to be more similar to that of R61.

CONCLUSIONS

The covalent adduct of the R61 DD-peptidase with the specific phosphonate inhibitor **2** mimics the structure of the transition state for formation of the tetrahedral intermediate in the deacylation step of the carboxypeptidase reaction. This interpretation identifies the Tyr159 anion as the general base catalyst of water attack on the acyl−enzyme intermediate. Lys65 would then act as an electrostatic catalyst and hydrogen bond donor in this step. Comparisons of this crystal structure with previously determined structures of the Henri−Michaelis complex and the enzyme−products complex show that specific substrate binding induces a conformational change that positions Ser62 in an optimal position for catalysis. This activated conformation relaxes as catalysis proceeds. We have now succeeded in crystallographically imaging a covalent transition state analogue on the reaction pathway (Figure 6), adding to our understanding of the mechanism of action of this important class of enzymes, the targets of β-lactam antibiotics.

ACKNOWLEDGMENT

We acknowledge Jean-Marie Frère at Université of Liège for providing the R61 enzyme and Dieter Schneider and his staff at Brookhaven National Laboratory, National Synchrotron Light Source, beamline X12B (supported by the U.S. Department of Energy, Division of Materials Sciences and Division of Chemical Sciences, under Contract DE-AC02-98CH10886) for help in data collection.

REFERENCES

1. Spratt, B. G. (1975) Distinct penicillin binding proteins involved in the division, elongation, and shape of *Escherichia coli* K12, *Proc. Natl. Acad. Sci. U.S.A. 72*, 2999−3003.
2. Koch, A. L. (2000) Penicillin binding proteins, β-lactams, and lactamases: offensives, attacks, and defensive countermeasures, *Crit. Rev. Microbiol. 26*, 205−220.
3. Tipper, D. J., and Strominger, J. L. (1965) Mechanism of action of penicillins: a proposal based on their structural similarity to acyl-D-alanyl-D-alanine, *Proc. Natl. Acad. Sci. U.S.A. 54*, 1133−1141.
4. Frere, J. M., and Joris, B. (1985) Penicillin-sensitive enzymes in peptidoglycan biosynthesis, *CRC Crit. Rev. Microbiol. 11*, 299−396.
5. Kelly, J. A., Knox, J. R., Moews, P. C., Hite, G. J., Bartolone, J. B., Zhao, H., Joris, B., Frere, J.-M., and Ghuysen, J.-M. (1985) 2.8 Å structure of penicillin-sensitive DD-peptidase from *Streptomyces* R61 and complexes with β-lactams, *J. Biol. Chem. 260*, 6449−6458.
6. Anderson, J. W., and Pratt, R. F. (2000) Dipeptide binding to the extended active site of the *Streptomyces* R61 D-alanyl-D-alanine peptidase: The path to a specific substrate, *Biochemistry 39*, 12200−12209.
7. McDonough, M., Anderson, J., Silvaggi, N., Pratt, R., Knox, J., and Kelly, J. (2002) Structures of Two Kinetic Intermediates Reveal Species Specificity of Penicillin-binding Proteins, *J. Mol. Biol. 322*, 111−122.
8. Rahil, J., and Pratt, R. F. (1991) Phosphonate monoester inhibitors of class A β-lactamases, *Biochem. J. 275*, 793−795.
9. Markowska, A., Olejnik, J., Mlotkowska, B., and Sobanska, M. (1981) *Phosphorus Sulfur 10*, 143−146.
10. Ho, G.-J., Emerson, K. M., Mathre, D. J., Shuman, R. F., and Grabowski, E. J. J. (1995) *J. Org. Chem. 60*, 3569−3570.
11. Frere, J. M., Leyh-Bouille, M., Ghuysen, J. M., Nieto, M., and Perkins, H. R. (1976) Exocellular DD-carboxypeptidases-transpeptidases from *Streptomyces*, *Methods Enzymol. 45*, 610−636.
12. Bernstein, J., and Pratt, R. (1999) On the importance of a methyl group in β-lactamase evolution: Free energy profiles and molecular modeling, *Biochemistry 38*, 10499−10510.

13. Pratt, R. F., McConnell, T. S., and Murphy, S. J. (1988) Accumulation of an acyl-enzyme intermediate during turnover of penicillin by the class A β-lactamase of *S. aureus* PC1, *Biochem. J. 254*, 919−922.
14. Otwinowski, Z., and Minor, W. (1997) Processing of X-ray diffraction data collected in oscillation mode, *Methods Enzymol. 276*, 307−326.
15. Brunger, A. T., Adams, P. D., Clove, G. M., Delano, W. L., Gros, P., Grosse-Kunstleve, R. W., Jiang, J.-S., Kuszewski, J., Nilges, M., Pannu, N. S., Read, R. J., Rice, L. M., Simonson, T., and Warren, G. L. (1998) CNS (Crystallography and NMR System), *Acta Crystallogr. D54*, 905−921.
16. McRee, D. E. (1999) XtalView/Xfit: A versatile program for manipulating atomic coordinates and electron density, *J. Struct. Biol. 125*, 156−165.
17. Sheldrick, G. M., and Schneider, T. R. (1997) SHELXL: high-resolution refinement, *Methods Enzymol. 277*, 319−343.
18. Knox, J. R., Moews, P. C., and Frere, J.-M. (1996) Molecular evolution of bacterial β-lactam resistance, *Chem. Biol. 3*, 937−947.
19. Rahil, J., and Pratt, R. F. (1992) Mechanism of inhibition of the class C β-lactamase of *Enterobacter cloacae* P99 by phosphonate monoesters, *Biochemistry 31*, 5869−5878.
20. Li, N., Rahil, J., Wright, M. E., and Pratt, R. F. (1997) Structure−activity studies of the inhibition of serine β-lactamases by phosphonate monoesters, *Bioorg. Med. Chem. 5*, 1783−1788.
21. Xu, Y., Soto, G., Adachi, H., van der Linden, M. P. G., Keck, W., and Pratt, R. F. (1994) Relative specificities of a series of β-lactam-recognizing enzymes towards the side-chains of penicillins and of acyclic thioldepsipeptides, *Biochem. J. 302*, 851−856.
22. Murphy, B. P., and Pratt, R. F. (1991) N-(Phenylacetyl)glycyl-D-aziridine-2-carboxylate, an acyclic amide substrate of β-lactamases: Importance of the shape of the substrate in β-lactamase evolution, *Biochemistry 30*, 3640−3649.
23. Lobkovsky, E., Billings, E. M., Moews, P. C., Rahil, J., Pratt, R. F., and Knox, J. R. (1994) Crystallographic structure of a phosphonate derivative of the *Enterobacter cloacae* P99 cephalosporinase: Mechanistic interpretation of a β-lactamase transition state analog, *Biochemistry 33*, 6762−6772.
24. Pauling, L. (1960) *The Nature of the Chemical Bond*, 3rd ed., Cornell University Press, Ithaca, NY.
25. Kelly, J. A., and Kuzin, A. P. (1995) Refined crystallographic structure of a DD-peptidase penicillin target enzyme at 1.6 Å resolution, *J. Mol. Biol. 254*, 223−236.
26. Wilkin, J.-M., Dubus, A., Joris, B., and Frere, J.-M. (1994) The mechanism of action of DD-peptidases: the role of Thr-299 and -301 in the *Streptomyces* R61 DD-peptidase, *Biochem. J. 301*, 477−483.
27. Hadonou, A. M., Wilkin, J.-M., Varetto, L., Joris, B., Lamotte-Brasseur, J., Klein, D., Duez, C., Ghuysen, J.-M., and Frere, J.-M. (1992) Site-directed mutagenesis of the *Streptomyces* R61 DD-peptidase, *Eur. J. Biochem. 207*, 97−102.
28. Wilkin, J.-M., Jamin, M., Damblon, C., Zhao, G.-H., Joris, B., and Frere, J.-M. (1993) The mechanism of action of DD-peptidases: the role of tyrosine-159 in the *Streptomyces* R61 DD-peptidase, *Biochem. J. 291*, 537−544.
29. Massova, I., and Mobashery, S. (1998) Kinship and diversification of bacterial penicillin-binding proteins and β-lactamases, *Antimicrob. Agents Chemother. 42*, 1−17.
30. Koshland, D. E., Jr. (1958) Application of a theory of enzyme specificity to protein synthesis, *Proc. Natl. Acad. Sci. U.S.A. 44*, 98−123.
31. Kelly, J. A., Dideberg, O., Charlier, P., Wery, J.-P., Libert, M., Moews, P. C., Knox, J. R., Duez, C., Fraipont, C., Joris, B., Dusart, J., Frere, J.-M., and Ghuysen, J.-M. (1986) On the origin of bacterial resistance to penicillin: Comparison of a β-lactamase and a penicillin target, *Science 231*, 1429−1431.
32. Samraoui, B., Sutton, B. J., Toddy, R. J., Artymiuk, P. J., Waley, S. G., and Phillips, D. C. (1986) Tertiary structural similarity between a class A β-lactamase and a penicillin-sensitive D-alanyl carboxypeptidase-transpeptidase, *Nature 320*, 378−380.
33. Lobkovsky, E., Moews, P. C., Liu, H., Zhao, H., Frere, J.-M., and Knox, J. R. (1993) Evolution of an enzyme activity: Crystallographic structure at 2 Å resolution of the cephalosporinase from the *ampC* gene of *Enterobacter cloacae* P99 and comparison with a class A penicillinase, *Proc. Natl. Acad. Sci. U.S.A. 90*, 11257−11261.
34. Joris, B., Ledent, P., Dideberg, O., Fonze, E., Lamotte-Brasseur, J., Kelly, J. A., Ghuysen, J.-M., and Frere, J.-M. (1991) Comparison of the sequences of class A β-lactamases and the secondary structure elements of penicillin-recognizing proteins, *Antimicrob. Agents Chemother. 35*, 2294−2301.
35. Luzzati, V. (1952) Traitement statisque des erreurs dans la détermination des structures cristallines, *Acta Crystallogr. 5*, 802−810.
36. Merrit, E. A., and Bacon, D. J. (1997) Raster3D: Photorealistic molecular graphics, *Methods Enzymol. 277*, 505−524.
37. Kraulis, P. (1991) MOLSCRIPT: a program to produce both detailed and schematic plots of protein structures, *J. Appl. Crystallogr. 24*, 946−950.
38. Carson, M. (1997) Ribbons, *Methods Enzymol. 277*, 493−505.

BI0268955